Time History of Events and Macroscale Interactions during Substorms observations of a series of hot flow anomaly events

H. Zhang,[1,2] D. G. Sibeck,[1] Q.-G. Zong,[3] S. P. Gary,[4] J. P. McFadden,[5] D. Larson,[5] K.-H. Glassmeier,[6] and V. Angelopoulos[7]

Received 9 December 2009; revised 25 September 2010; accepted 6 October 2010; published 15 December 2010.

[1] A series of seven hot flow anomaly (HFA) events has been observed by the Time History of Events and Macroscale Interactions during Substorms (THEMIS) C spacecraft just upstream from the subsolar bow shock from 0100 to 1300 UT on 19 August 2008. Both young (no shocks at edges, two distinct ion populations) and mature (strong shocks at edges, a single hot ion population) HFAs have been observed. Further upstream, THEMIS B observed four proto-HFAs (density and magnetic field strength depletions, plasma heating but no flow deflections) which later developed into HFAs observed by THEMIS C. We present evidence indicating that electromagnetic right-hand resonant ion beam instabilities heat ions inside HFAs. Observations of small-amplitude perturbations ($\Delta B/B < 50\%$) consistent with the resonant ion beam instability in a proto-HFA, 30 s electromagnetic waves ($\Delta B/B \sim 1$) in a young HFA, and magnetic pulsations in a mature HFA ($\Delta B/B \sim 4$) indicate that they are at early, middle, and late (nonlinear) stages of the electromagnetic right-hand resonant ion beam instabilities. Both young and mature HFAs are associated with strong electromagnetic waves near the lower hybrid frequency (0.1–1 Hz). The lower hybrid waves are the likely source of the electron heating inside HFAs. THEMIS B observations of four proto-HFAs which later developed into HFAs observed by THEMIS C indicate that these four HFAs might extend beyond 14 R_E upstream from the bow shock, while the other three HFAs may extend between 5 and 14 R_E upstream from the bow shock. We present an example of an HFA that lies displaced toward the side of the tangential discontinuity with a quasi-parallel bow shock configuration rather than lying centered on the driving interplanetary magnetic field discontinuity.

Citation: Zhang, H., D. G. Sibeck, Q.-G. Zong, S. P. Gary, J. P. McFadden, D. Larson, K.-H. Glassmeier, and V. Angelopoulos (2010), Time History of Events and Macroscale Interactions during Substorms observations of a series of hot flow anomaly events, *J. Geophys. Res.*, *115*, A12235, doi:10.1029/2009JA015180.

1. Introduction

[2] Hot flow anomalies (HFAs) are events observed near the bow shock that are marked by greatly heated solar wind plasmas and substantial flow deflection [e.g., *Schwartz*, 1995]. The ion temperature inside HFAs is typically about an order of magnitude above the electron temperature (Ti ~ 10^7K and Te ~ 10^6K), and the plasma flow speed in HFAs typically ranges from about 20% to 50% of the solar wind speed [*Onsager et al.*, 1990]. The hot tenuous plasma is usually bounded by regions of enhanced magnetic field strength and density. The outer edges of these enhancements are fast shocks. The inner edges are tangential discontinuities which separate the dense "sheath" population from the tenuous and hot plasma at the center of the HFA. Some HFAs show magnetic field and density enhancement only on the trailing edge [e.g., *Schwartz*, 1995].

[3] HFAs are thought to be produced by the interaction of certain upstream discontinuities with the bow shock [*Thomas et al.*, 1991]. Figure 1 shows a schematic plot for the structure of an HFA event standing upstream from the bow shock. Ions reflected from the bow shock are energized and trapped in the vicinity of the discontinuities when the motional electric fields (**E**) point toward the discontinuity. The ions are thermalized by encounters with the bow shock, creating a high-pressure plasma near the intersection of the bow shock and the current sheet. The regions of high

[1]NASA Goddard Space Flight Center, Greenbelt, Maryland, USA.
[2]Geophysical Institute, University of Alaska Fairbanks, Fairbanks, Alaska, USA.
[3]Center for Atmospheric Research, University of Massachusetts Lowell, Lowell, Massachusetts, USA.
[4]Space Science and Applications, Los Alamos National Laboratory, Los Alamos, New Mexico, USA.
[5]Space Sciences Laboratory, University of California, Berkeley, California, USA.
[6]Institute for Geophysics and Extraterrestrial Physics, Technische Universität Braunschweig, Braunschweig, Germany.
[7]Institute of Geophysics and Planetary Physics, Department of Earth and Space Sciences, University of California, Los Angeles, California, USA.

Copyright 2010 by the American Geophysical Union.
0148-0227/10/2009JA015180

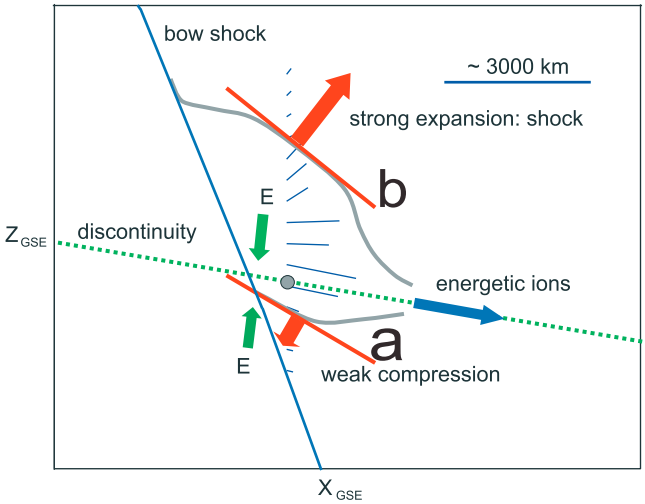

Figure 1. Schematic plot of an HFA event showing its structure formed by the interaction of interplanetary discontinuity with the Earth's bow shock [*Lucek et al.*, 2004].

temperature then expand against the surrounding medium, leading to a low density and magnetic field strength core flanked by regions of enhanced magnetic field strength and density. Observations indicate that HFA events are associated with current sheets exhibiting the predicted inward electric field orientation on at least one side [*Thomsen et al.*, 1993]. High solar wind speeds favor the formation of HFAs [*Facskó et al.*, 2008, 2009a].

[4] HFAs evolve and grow with time. HFAs containing two ion populations, a solar wind beam and a reflected ion distribution, have been observed [*Thomsen et al.*, 1986, 1988; *Lucek et al.*, 2004; *Eastwood et al.*, 2008] and the presence of two populations has been interpreted as the signature of an HFA at an early stage of evolution [*Thomsen et al.*, 1988; *Lucek et al.*, 2004] or relatively young [*Eastwood et al.*, 2008].We call such events "young HFAs" [*Lucek et al.*, 2004; *Tjulin et al.*, 2008] throughout the remainder of this paper. The ion distributions inside HFAs at later stages show a single hot isotropic Maxwellian distribution [*Thomsen et al.*, 1986; *Lucek et al.*, 2004]. We call these events "mature HFAs" throughout the remainder of this paper. The electron distributions inside mature HFAs are isotropic and can be reasonably well fit by a Maxwellian function over the lower-energy portion of the spectrum [*Thomsen et al.*, 1986, 1988].

[5] One outstanding question concerns how ions and electrons are heated inside HFAs. Two types of approaches have been taken to explain the ion heating inside HFAs. In the hybrid simulation of *Thomas et al.* [1991], ions reflected from the bow shock are accelerated toward the current sheet of the discontinuity by the motional electric field. These ions are then scattered by subsequent encounters with the shock and/or the current sheet (no instability is involved), producing the high ion temperature within HFAs. In this scenario, strong coupling between the two ion components is not fully described [*Schwartz*, 1995]. In a different approach, *Thomsen et al.* [1988] suggested that the high ion temperatures within HFAs are produced by strong coupling between dense shock-reflected ions and the incident solar wind ions mediated by an electromagnetic right-hand nonresonant ion beam instability. Two-dimensional hybrid simulations by *Thomas and Brecht* [1988] showed that the interaction between an ion beam of finite extent and a background plasma can produce many features similar to those observed in HFAs through a right-hand resonant ion beam instability. A one-dimensional hybrid simulation by *Onsager et al.* [1991] showed that both the nonresonant and resonant modes contribute to the beam coupling. Electron heating inside HFAs has received less attention.

[6] In 2-D hybrid simulations [*Lin*, 2002], the size of HFAs in the solar wind depends on the rotation angle of the magnetic field through the tangential discontinuity and the orientation of the discontinuity. The size of HFAs increases with the rotation angle of the magnetic field through the tangential discontinuity (TD). It also increases with the angle γ between the TD normal and the Sun-Earth line. It reaches a maximum at $\gamma \sim 80°$. A statistical study of 124 Cluster HFAs showed that the average value for the rotation angle of the magnetic field through the TD was 70° and the angle between the solar direction and the TD normal was larger than 45° [*Facskó et al.*, 2009a, 2009b] which is consistent with simulation results by *Lin* [2002]. The thickness of HFAs in the direction of motion is of the order of a few Earth radii R_E [e.g., *Schwartz et al.*, 1985; *Thomsen et al.*, 1986; *Sibeck et al.*, 1999; *Lucek et al.*, 2004; *Facskó et al.*, 2009a, 2009b]. The second outstanding problem is how far HFAs extend upstream from the bow shock. *Woolliscroft et al.* [1986] inferred that one HFA extended no more than several R_E upstream from the bow shock by noting the absence of this event further upstream despite an observation of the same interplanetary current sheet.

[7] The third outstanding problem is where HFAs occur. Simulations and observations show completely different results on whether HFAs occur at quasi-perpendicular or quasi-parallel shocks. Hybrid simulations by *Thomas et al.* [1991] demonstrated the formation of HFAs by the interaction of a tangential discontinuity with a planar quasi-perpendicular shock. Using a global hybrid code, *Lin* [2002] showed that HFAs form in the quasi-perpendicular shock region. On the other hand, Figure 2 shows an example of an HFA that formed on the quasi-parallel side of an interplanetary magnetic field (IMF) discontinuity intersecting the bow shock [*Omidi and Sibeck*, 2007]. Observationally, *Thomsen et al.* [1988] found that HFAs tend to occur near the transition region between the quasi-perpendicular and quasi-parallel shock. Based on a study of 30 HFAs, *Schwartz et al.* [2000] found quasi-perpendicular shock conditions on at least one side of most HFAs, although several HFAs correspond to quasi-parallel conditions on both sides. *Facskó et al.* [2009a] observed 66% of 124 HFAs in the quasi-parallel region supporting the simulation of *Omidi and Sibeck* [2007].

[8] In this paper, we present Time History of Events and Macroscale Interactions during Substorms (THEMIS) observations of a series of seven HFAs and associated proto-HFAs upstream from the bow shock. A proto-HFA (or HFA to be) is a structure which later develops into an HFA. A proto-HFA is characterized by decreases in the magnetic field strength and plasma density, moderate ion and electron heating, and turbulent but not deflected solar wind flow (see section 3.1 for details). We present particle

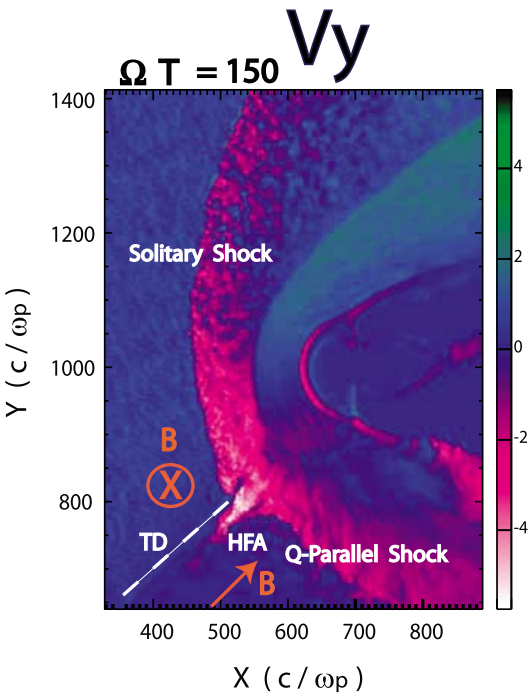

Figure 2. Hybrid simulation showing the formation of an HFA via the interaction of an interplanetary tangential discontinuity (the white dashed line marked by TD) with the Earth's bow shock [*Omidi and Sibeck*, 2007]. The color contours show the Y component of the ion velocity. The HFA lies displaced toward the side of the TD with a quasi-parallel bow shock configuration instead of lying centered on the driving IMF TD.

distributions and wave observations inside proto-HFA, young and mature HFAs and propose that electromagnetic right-hand resonant ion beam instabilities are sources of ion heating inside HFAs. Both young and mature HFAs are associated with strong electromagnetic waves near the lower hybrid frequency (0.1–1 Hz). The lower hybrid waves are the likely source of the electron heating inside HFAs. THEMIS B observations of four proto-HFAs which later developed into HFAs observed by THEMIS C indicate that these four HFAs might extend beyond 14 R_E upstream from the bow shock, while the other three HFAs may extend between 5 and 14 R_E upstream from the bow shock. We also show an example which agrees very well with results from a hybrid simulation by *Omidi and Sibeck* [2007] indicating that HFAs lie displaced toward the quasi-parallel side of TDs instead of lying centered on the driving IMF discontinuity.

[9] The plasma observations reported in this paper were obtained by the electrostatic analyzer (ESA) [*McFadden et al.*, 2008] on the THEMIS spacecraft [*Angelopoulos*, 2008]. In one 3 s spin, ESA measures the 3-D ion and electron distributions over the energy range from a few eV up to 30 keV for electrons and 25 keV for ions. ESA data are formatted into four modes with different time resolution, solid angle and/or energy coverage. Burst modes contain spin resolution 3-D plasma distributions with 32 energies and 88 solid angles. Due to telemetry limitations, burst modes are generally limited to several 5 min intervals each orbit. We are lucky that burst mode data are available during the time interval of HFA 7. Reduced modes are also a spin resolution data product, but with limited solid angle and/or energy coverage (24 energies, 50 solid angles for ions and 32 energies, 6 solid angles for electrons in a fast survey mode). Full modes are a low time resolution (32 spins in a

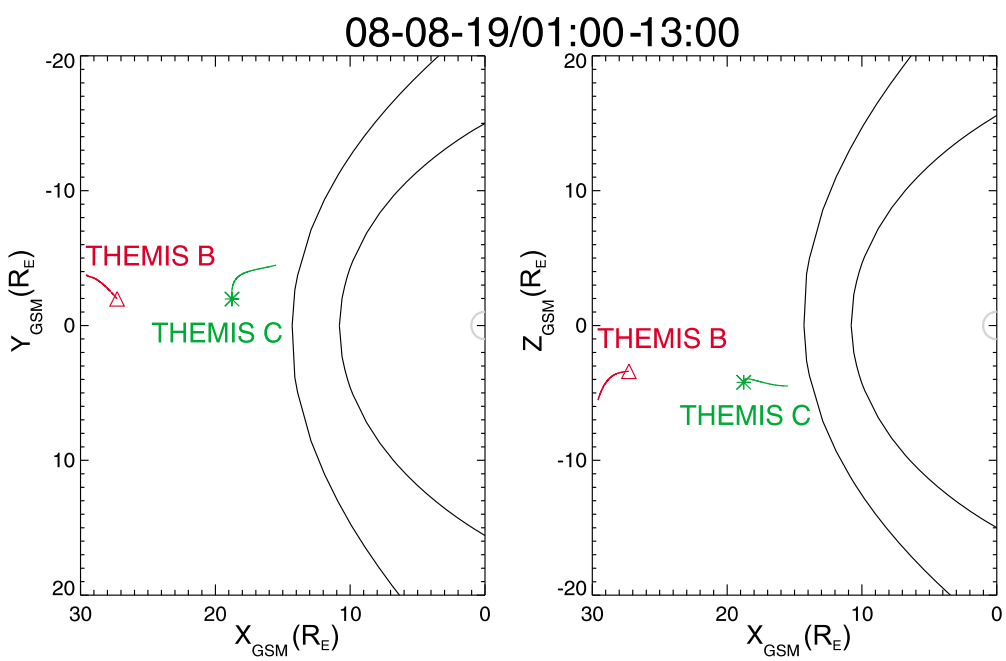

Figure 3. THEMIS trajectory projected in GSM (left) X–Y plane and (right) X–Z plane from 0100 to 1300 UT on 19 August 2008. The positions of THEMIS B and C probes at 1300 UT are marked by a red triangle and green asterisk, respectively. During this 12 h time interval, both THEMIS B and C were upstream of the bow shock.

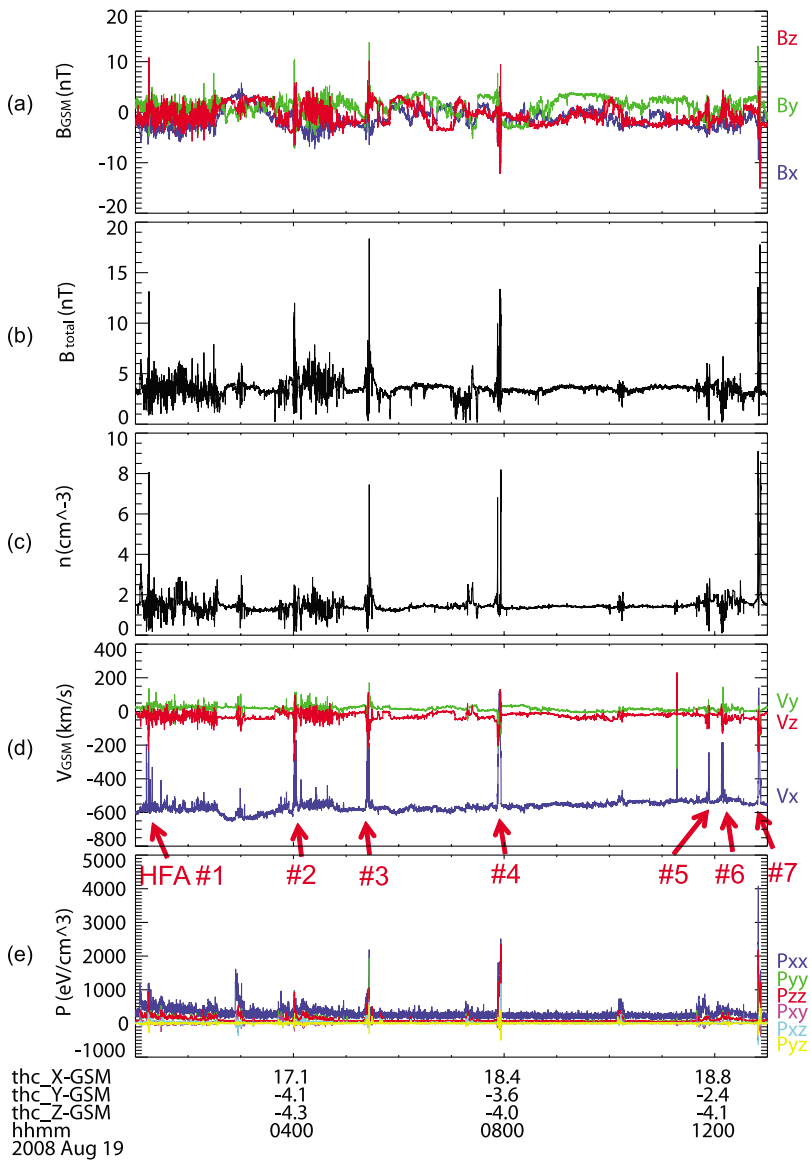

Figure 4. An overview plot of THEMIS C observations of a serious of seven HFAs upstream from the bow shock. (a) Components of the magnetic field in GSM coordinate system, (b) magnetic field magnitude, (c) plasma ion density (in cm^{-3}), (d) components of plasma ion flow, and (e) plasma ion pressure are shown.

fast survey mode or 128 spins in a slow survey mode) data product with full 32 energies and 88 solid angles. Onboard moments contain spin resolution on-board computations of the ion and electron ESA and the SST (>30 keV) moments. The magnetic field observations presented herein are from the fluxgate magnetometer (FGM) [*Auster et al.*, 2008] which measures the DC magnetic field up to 128 Hz.

2. Observations

[10] Figure 3 shows the trajectory of the THEMIS spacecraft [*Angelopoulos*, 2008] from 0100 to 1300 UT on 19 August 2008. THEMIS B and C were upstream from the bow shock. A red triangle and a green asterisk mark the positions of B (red) and C (green). The positions of probes are 14 R_E and 5 R_E upstream from the bow shock at 1300 UT. THEMIS A, D, and E were in the magnetosphere during this time interval (not shown).

2.1. THEMIS C Observations

[11] THEMIS C observed a series of seven HFAs from 0100 to 1300 UT on 19 August 2008. Figure 4 shows an overview plot of these seven HFAs. Figure 4a shows the three components of the magnetic field in the GSM coordinate system as measured by FGM instrument. Figure 4b shows the magnetic field strength. Figures 4c–4e show the plasma ion density, components of the plasma flow and pressure tensor observed by the ESA instrument. Clear flow deflections mark the seven HFAs identified by arrows in Figure 4d.

[12] We were struck by the fact that seven HFAs occurred in 12 h, far more frequently than the estimated rate of three

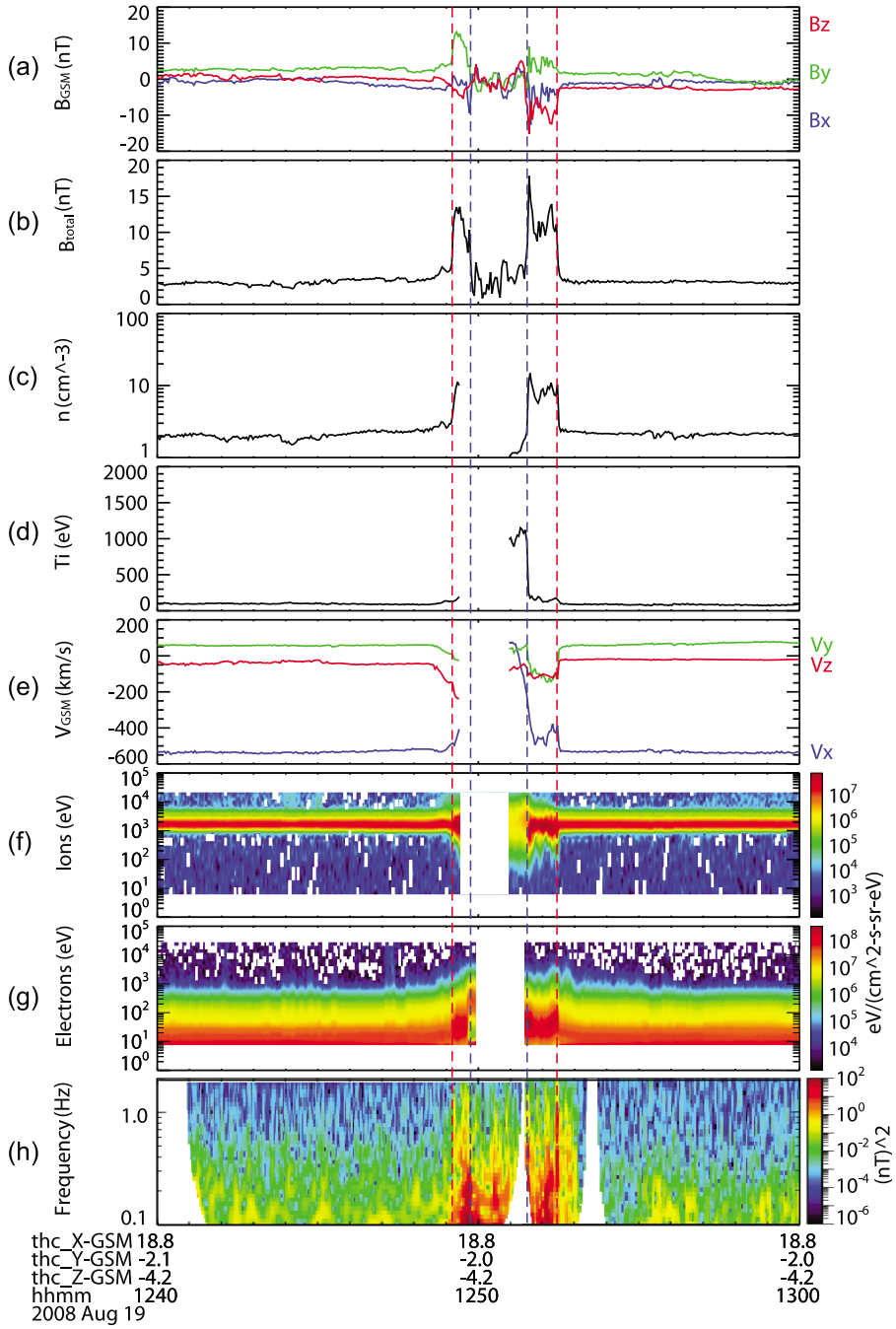

Figure 5. An overview plot of THEMIS C observations of a mature HFA (HFA 7) upstream from the bow shock. (a) Components of the magnetic field in GSM coordinate system, (b) magnetic field magnitude, (c) plasma ion density, (d) plasma ion temperature, (e) components of plasma flow, (f) plasma ion spectrum, (g) plasma electron spectrum, and (h) the wavelet analysis result for the B_x component of the magnetic field are shown. The vertical red dashed lines at 1249:10 and 1252:25 UT mark the shocks on both edges of HFA. The vertical blue dashed lines at 1249:45 and 1251:30 UT mark the discontinuities which separate the dense sheath population from the tenuous plasma at the center of the HFA.

events per day by *Schwartz et al.* [2000]. It is clear that the conditions on this day must have been very conducive to HFA formation. As noted by *Facskó et al.* [2008], a high solar wind speed favors the formation of HFAs. Figure 4d confirms that the solar wind speed was indeed high on this day at 600 km/s.

[13] Figure 5 shows a mature HFA observed by THEMIS C upstream from the bow shock at 1250 UT. The time interval shown is 20 minutes. This was the final HFA in the sequence of seven shown in Figure 4. Figure 5a shows FGM observations of the three components of the magnetic field in the GSM coordinate system with 3 s time resolution.

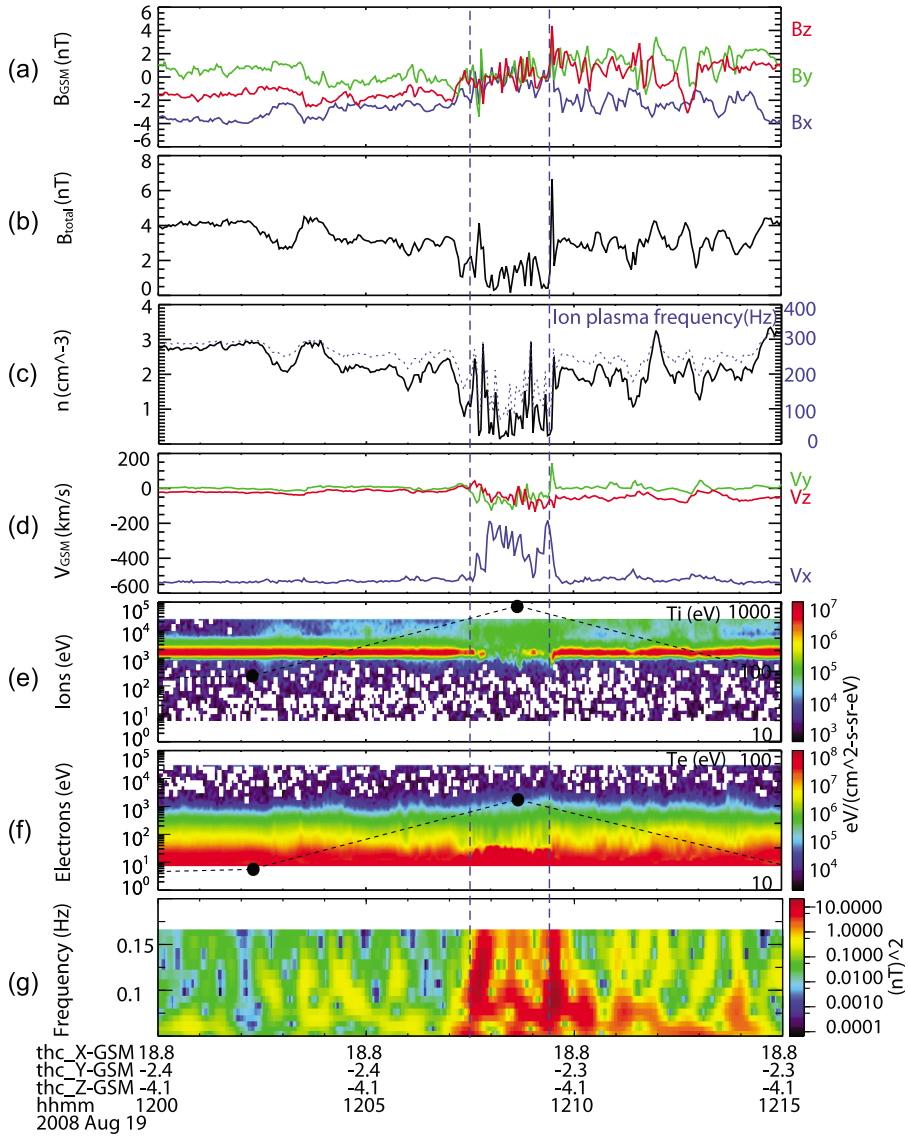

Figure 6. An overview plot of THEMIS C observations of a young HFA (HFA 6). (a) Components of the magnetic field in GSM coordinate system, (b) magnetic field magnitude, (c) plasma ion density, (d) components of plasma flow, (e) plasma ion spectrum, (f) plasma electron spectrum, and (g) the wavelet analysis result for the B_x component of the magnetic field (the cut at 0.17 Hz is due to the 3s resolution of the magnetic field measurement) are shown. The vertical blue dashed lines at 1207:30 and 12:09:30 UT mark edges of the HFA. The plasma ion frequency is overplotted by a blue dashed line and using the right-hand axis in Figure 6c. The ion (electron) temperature is overplotted in black dots and using the right-hand axis in Figure 6e (Figure 6f).

Figure 5b shows the magnetic field strength. Figures 5c–5e show the plasma ion density, temperature and components of the plasma flow obtained by the ESA plasma analyzer with 3s time resolution. Figures 5f and 5g show the ESA plasma ion spectra and ESA electron spectra. Figure 5h shows the wavelet analysis result for the B_x component of the magnetic field. Weak and variable magnetic field strengths (Figure 5b) indicate the core region at the center of the HFA from 1249:45 to 1251:30 UT (marked by vertical dashed blue lines). Although there is a data gap in plasma observations within this region, those plasma observations that are available indicate reduced densities (Figure 5c) and enhanced temperatures (Figures 5d, 5f, and 5g). Regions of enhanced magnetic field strength and density from 1249:10 to 1249:45 and 1251:30 to 1252:25 UT bound this core region. The outer edges of these enhancements, which are marked by vertical red dashed lines at 1249:10 UT and 1252:25 UT, are fast shocks because they are characterized by increases in solar wind density, temperature, velocity and the magnitude of the magnetic field. The inner edges, which are marked by vertical blue dashed lines at 1249:45 UT and 1251:30 UT, are tangential discontinuities which separate the dense ($n \sim 10cm^{-3}$) sheath population from the tenuous ($n \sim 1cm^{-3}$) and hot ($Ti \sim 10^7K$) plasma at the center of the HFA. The fast shocks at the edges of the HFA (together with the hot single ion population shown in Figure 7a) indicate

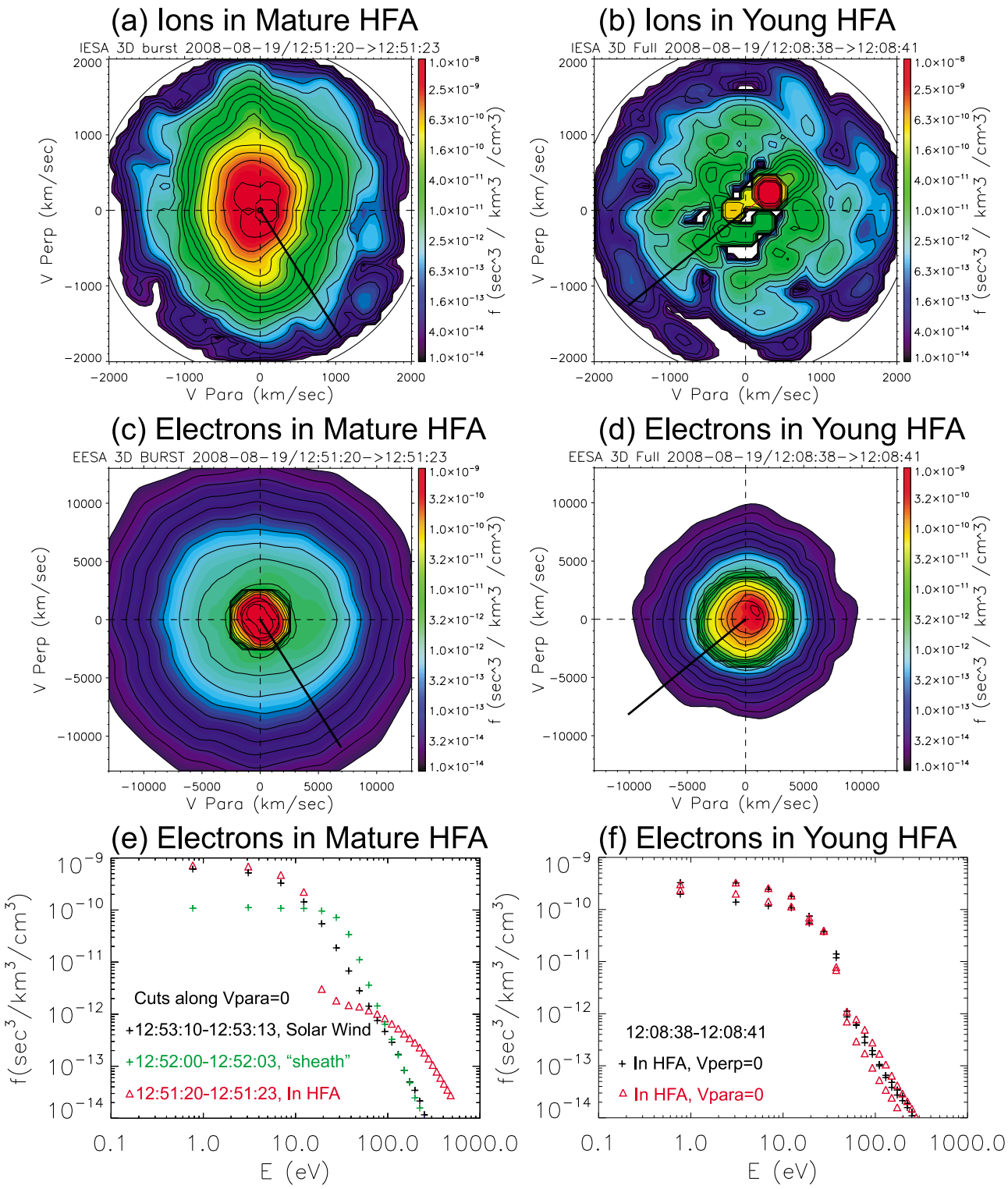

Figure 7. Ion and electron distribution recorded by THEMIS C at the center of a mature (HFA 7) and young (HFA 6) HFA. Ion distribution inside a (a) mature and (b) young HFA. Electron distribution inside a (c) mature (HFA 7) and (d) young (HFA 6) HFA. The thick black lines point toward the sun. (e) One-dimensional cuts of electron distributions in the solar wind (black crosses), in the sheath region (green crosses) and at the center (red triangles) of a mature HFA. (f) One-dimensional cut plot of the electron distribution inside a young HFA (shown in Figure 7d). The black crosses (red triangles) show the cut along Vperp = 0 (Vpara = 0).

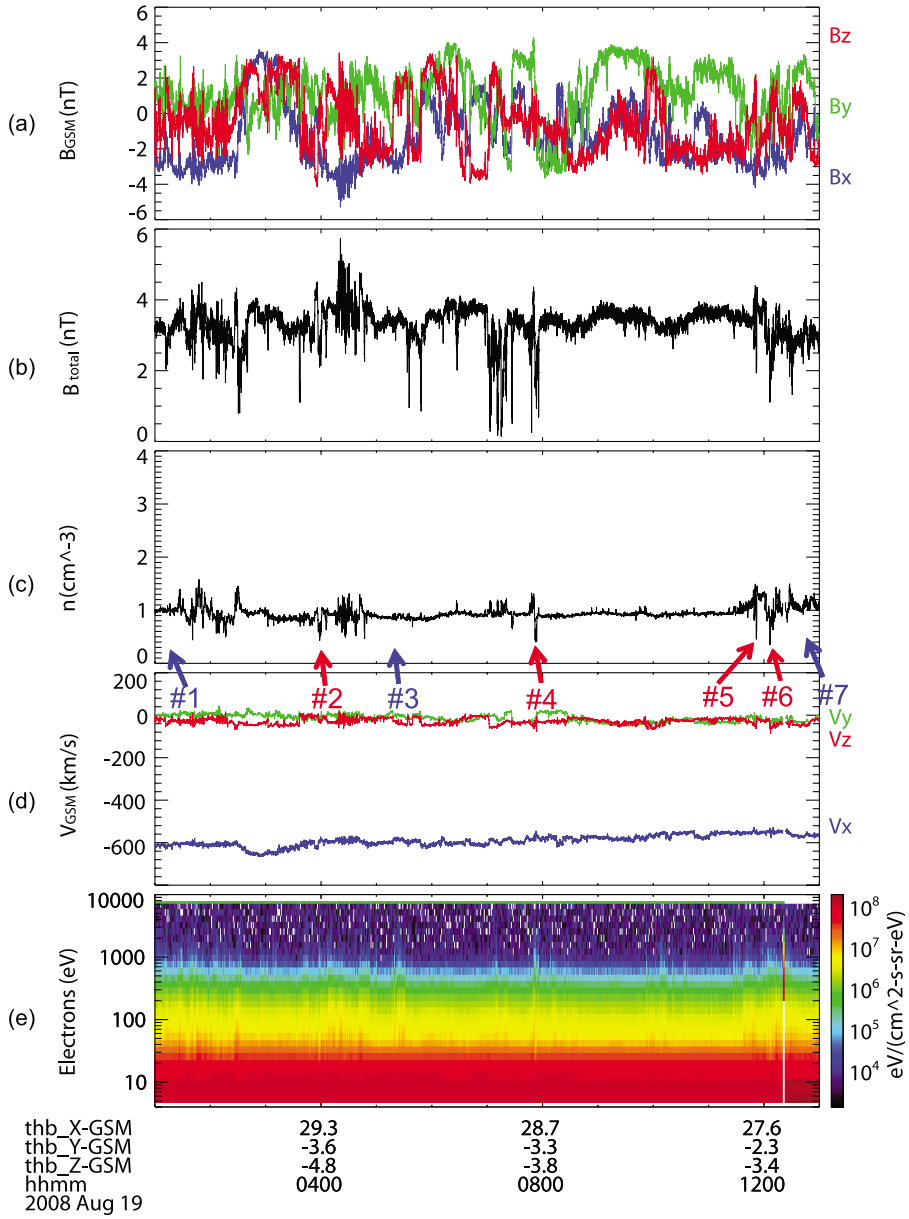

Figure 8. An overview plot of THEMIS B observations upstream from the bow shock. The time interval is the same as that of Figure 4. (a) Components of the magnetic field in GSM coordinate system, (b) magnetic field magnitude, (c) plasma density (in cm^{-3}), (d) components of plasma flow, and (e) plasma electron spectrum are shown. The onboard moments shown in Figure 8d (and Figure 9d (left)) are rescaled to match the ground calibrated data. (We expect the corrections to be applied in the near future.)

that the HFA is well developed or mature. THEMIS C observed strong electromagnetic waves near the lower hybrid frequency (0.1–1 Hz) in the mature HFA (Figure 5h). Low hybrid waves is one of the possible interpretation of observed waves.

[14] Figure 6 shows a young HFA (HFA 6) that THEMIS C observed about 40 mins prior to HFA 7. It is characterized by a significant deflection in the plasma velocity (Figure 6d), together with reduced magnetic field strength (Figure 6b), reduced density (Figure 6c) and plasma heating (Figure 6e) from 1207:30 and 1209:30 UT. But no clear shocks are observed on either edge. There was strong electromagnetic wave activity near the lower hybrid frequency (0.05–0.17 Hz) in the young HFA (Figure 6g). Low hybrid waves is one of the possible interpretation of observed waves.

[15] Figure 7 compares ion and electron distribution recorded by THEMIS C at the center of the mature (HFA 7) and young (HFA 6) HFAs. Figures 7a and 7b show ion distributions inside the mature and young HFAs, respectively. The ion distribution inside the mature HFA is an isotropic Maxwellian distribution which contains a single hot population. However two populations, an antisunward-propagating solar wind beam and a reflected ion beam centered on the $-V_{para}$ axis, were observed inside the young

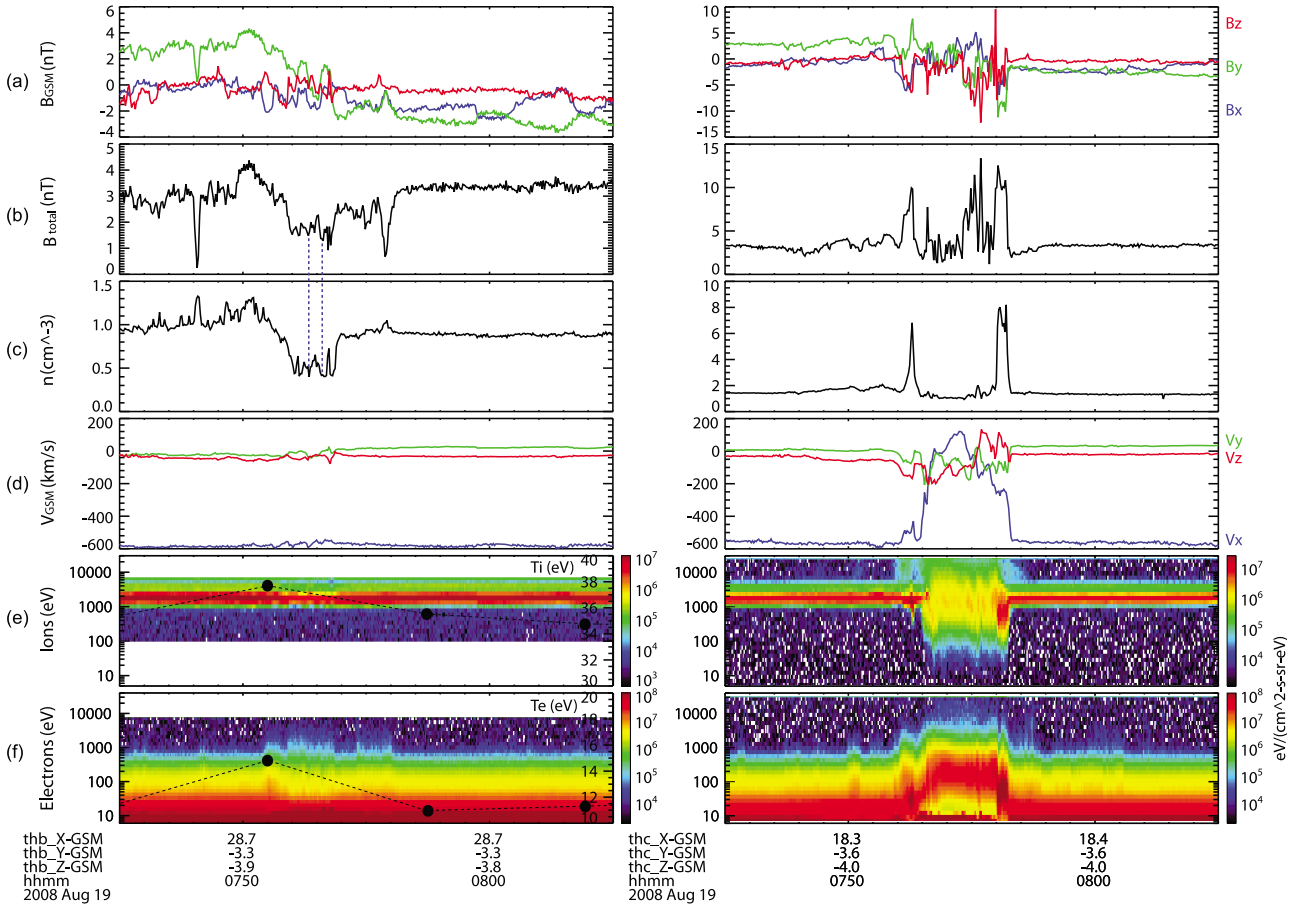

Figure 9. Comparison of THEMIS C observations of (right) HFA 4 and (left) the corresponding proto-HFA observed by THEMIS B upstream from the bow shock. (a) Components of the magnetic field in GSM coordinate system, (b) magnetic field magnitude, (c) plasma density (in cm^{-3}), (d) components of plasma ion flow, (e) plasma ion spectrum, and (f) plasma electron spectrum are shown. The ion (electron) temperature measured by THEMIS B is overplotted in black dots and using the right-hand axis in Figure 9e (Figure 9f).

HFA as shown in Figure 7b. Figures 7c and 7d show electron distributions inside mature (HFA 7) and young (HFA 6) HFAs, respectively. The electron distributions inside both HFAs are isotropic but electrons inside the mature HFA were much hotter than those in the young HFA as indicated by broader spacing. Figure 7e shows 1-D cuts of electron distributions taken in the solar wind (black crosses), in the sheath region (green crosses) and at the center (red triangles) of a mature HFA. Electron distributions taken in these three regions show very different signatures. The electron distribution taken in the solar wind is Maxwellian at lower energies. The distribution in the sheath region of the HFA exhibits the flattened top electron spectra characteristic of the Earth's magnetosheath [e.g., *Feldman et al.*, 1983]. By sharp contrast, the electron distribution at the center of the HFA shows a distinctively rounded shape at energies greater than 10 eV while maintaining the original solar wind distribution at energies below 10 eV. The electron distributions associated with HFAs have been reported by *Thomsen et al.* [1988]. They also showed the flattened top electron spectra in the compression region of HFAs and rounded shape electron spectra inside HFAs. Like *Thomsen et al.* [1988] we find rounded spectra shapes at energies greater than 10 eV. However, unlike them, we find a sharp jump in electron fluxes near 10 eV. The difference may be due to the narrower energy coverage (11 eV to 20 keV in the high-energy mode) of the FPE instrument onboard ISEE [*Thomsen et al.*, 1986]. Figure 7f shows a 1-D cut plot for electron distributions inside the young HFA (shown in Figure 7d). The black crosses (red triangles) show the cut along Vperp = 0 (Vpara = 0). The electron distribution inside the young HFA shows a Maxwellian distribution at lower energies and a power law tail.

[16] We have looked all seven HFAs. The characteristics of HFAs 1 and 4 are similar to the mature event shown in Figure 5 and those of HFAs 2, 3, and 5 are similar to the young HFA shown in Figure 6.

2.2. THEMIS B Observations

[17] As can be seen from Figure 3, THEMIS B was further upstream from the bow shock than THEMIS C. As an excellent solar wind monitor, THEMIS B observed all the undisturbed (or slightly disturbed where proto-HFAs were present) interplanetary current sheets (Figure 8a) associated with the THEMIS C HFAs. Although THEMIS B did not observe any significant deflections in the solar wind flow

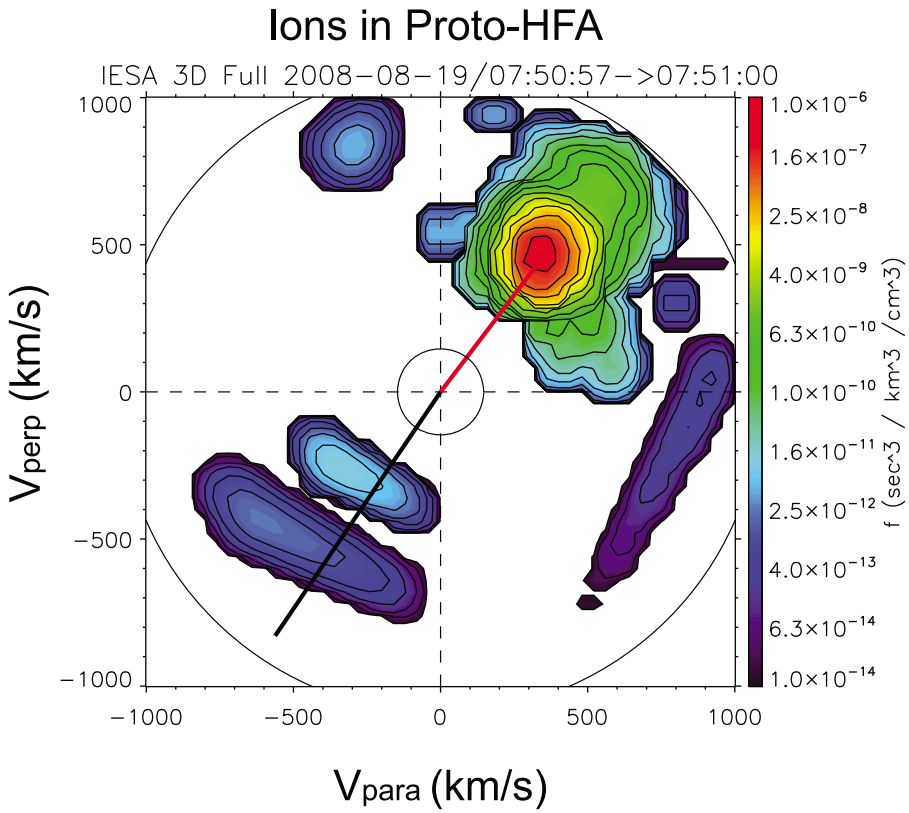

Figure 10. Ion distribution recorded by THEMIS B at the center of a proto-HFA. The thick black line points toward the sun and the thick red line points in the solar wind direction.

during this interval, it did observe density and magnetic field strength depletions (Figures 8b and 8c) and electron heating (Figure 8e) associated with interplanetary discontinuities that were observed at around 0357, 0752, 1150, and 1206 UT. These discontinuities generated HFAs 2, 4, 5, and 6 in Figure 4, respectively. Since density and magnetic field strength depletion and plasma heating are typical signatures of HFAs, we propose that these structures are proto-HFAs and they developed into HFAs 2, 4, 5, and 6 which were observed by THEMIS C downstream. We will compare signatures of HFA 4 and the corresponding proto-HFA observed by THEMIS B at around 0752 UT in section 3.

3. Discussion

3.1. Evolution of HFAs

[18] Figure 9 shows HFA 4 observed by THEMIS C (right) and the corresponding proto-HFA observed by THEMIS B (left). The magnetic fields recorded by THEMIS B and C are very similar (with 110 s time shift) except during the event time interval (Figure 9a). The proto-HFA observed by THEMIS B is characterized by decreases (~50%) in the magnetic field strength and plasma density (Figure 9b and 9c), moderate ion and electron heating (Figures 9e and 9f), and turbulent but not deflected solar wind flow (Figure 9d). After 110s, this proto-HFA developed into a mature HFA observed by THEMIS C. It has a very hot core (~10^7K) bounded by regions of strongly enhanced magnetic field strength and density. The magnetic fields were very turbulent inside the hot core but without much depletion in the field strength and plasma density (Figures 9b and 9c). The solar wind flow was significantly deflected (Figure 9d).

[19] Figure 10 shows the ion distribution at the center of the proto-HFA in Figure 9 (left). It contains two major ion populations, a solar wind beam (along the thick red line) and a reflected one (along the black line). No ion distribution functions were recorded in the center of the HFA shown in Figure 9 (right). Since this is a mature HFA with features similar to those shown in Figure 5, the ion distribution function should be similar to the one shown in Figure 7a which shows a single hot population. Therefore, we confirm *Thomsen et al.*'s [1988] suggestion that HFAs contain two ion populations, a solar wind beam and a reflected ion distribution, in their early stages. Later, strong coupling of these two ion populations converts the relative streaming energy of the two populations to the thermal energy of a single, hot, thermalized ion population [*Thomsen et al.*, 1988].

3.2. Particle Heating Inside HFAs

3.2.1. Ion Heating

[20] Efforts to describe how the interaction of the solar wind with a beam of reflected ions generate the high temperatures observed within HFAs have focused upon the electromagnetic right-hand ion instability. *Thomsen et al.* [1988] suggested that the coupling occurs via a nonresonant instability, while two-dimensional hybrid simulations reported by *Thomas and Brecht* [1988] showed that the

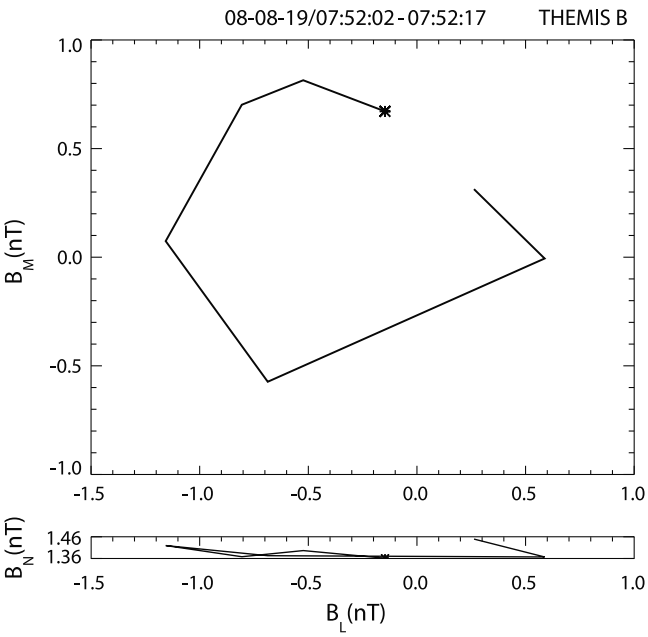

Figure 11. Hodogram of the time evolution (beginning with the asterisk) of the magnetic fields in the coordinate system determined from Minimum Variance Analysis (MVA) [*Sonnerup and Cahill*, 1967] for a 15 s segment of the data shown in Figure 9a (left). (top) Signal in the plane of the wave front and (bottom) sideways view of that plane. It is left-hand circular polarized in the spacecraft frame.

coupling occurs through a resonant ion beam instability. One dimensional hybrid simulations reported by *Onsager et al.* [1991] indicate both resonant and nonresonant modes contribute to the beam coupling. The right-hand resonant instability has often been invoked to explain large amplitude transverse compressive waves in the terrestrial foreshock [*Fairfield*, 1969; *Hoppe and Russell*, 1983; *Eastwood et al.*, 2004].

[21] Theory predicts that the resonant mode grows fastest when cold beam densities are less than 10% of those in the background plasma [*Gary*, 1991]. By contrast to the nonresonant instability, the resonant instability predicts strongly correlated magnetic field strength and plasma density fluctuations [*Akimoto et al.*, 1993]. It also predicts that the waves propagating parallel to the field-aligned ion beam will be right handed in the rest frame of the solar wind plasma [*Onsager et al.*, 1991]. Inspection of Figures 9b (left) and 9c (left) reveals positively correlated magnetic field strength and plasma density fluctuations within the proto-HFA from 0752–0754 UT, consistent with predictions for the resonant instability. To determine whether the waves are right handed, we must first identify the direction in which they are propagating and then their sense. We use minimum variance analysis [*Sonnerup and Cahill*, 1967] over the interval from 0752:02 to 0752:17 UT to obtain the minimum variance direction, which defines the direction of the wave vector (this direction has an ambiguity of 180°) and points antisunward in the GSE (x,y,z) = (−0.52, 0.60, 0.60) direction. This direction is well determined with a ratio of intermediate to minimum variance eigenvalues of 224. The mean magnetic field is determined by averaging the magnetic field vectors measured during this time interval and the direction of the mean field points antisunward in the GSE (x,y,z) = (−0.69, 0.63, 0.34) direction. The angle between the wave vector and the mean field is 18.9°, generally in agreement with the theory that the fastest growing waves propagate parallel to the ion beam, which in turn streams parallel or antiparallel to the magnetic field. The hodogram for the minimum versus maximum variance components shown in Figure 11 (bottom) demonstrates that the minimum variance component remains nearly constant at ~1.4 nT. The magnetic field perturbations associated with the wave lie in the plane perpendicular to the wave vector, as illustrated by the hodogram for the intermediate versus maximum variance components shown in Figure 11 (top). The reflected ion beam and the waves should propagate sunward, and therefore into the page. Inspection of Figure 11 (top) reveals that the waves are polarized left handed for this propagation direction. However, as noted by *Onsager et al.* [1991], removing the Doppler shift associated with the antisunward flowing solar wind results in right-handed waves in the rest frame of the solar wind plasma because the propagation speed of the waves predicted by linear theory is $\sim 2.8V_A = 103 km/s$, which is much slower than the solar wind speed ($\sim 600 km/s$). The wave length predicted by linear theory is $\sim 21 c/w_{pi} = 0.8 R_E$.

[22] The amplitude of the magnetic field and density fluctuations in the proto-HFA is relatively small (<50% of the background magnetic field). Young HFAs exhibit similar, but larger amplitude, fluctuations, as shown in Figure 12 which depicts HFA 5. During the event from 1150 to 1155 UT, the low-frequency (0.03 Hz) fluctuations occur mainly in the y and z components, perpendicular to the main magnetic field in the $-x$ direction. They are left-hand polarized in the spacecraft frame (not shown). The magnetic field magnitude and the plasma density are positively correlated. The amplitude of the magnetic fluctuation is ~4 nT, comparable to the background magnetic field strength (~4 nT). These signatures indicate that they are low- frequency (0.03 Hz in the spacecraft frame), large-amplitude ($\Delta B/B \sim 1$), transverse compressive electromagnetic waves. These waves have been observed in the terrestrial foreshock and are thought to be generated by back-streaming ions through the ion-ion right-hand instability [*Fairfield*, 1969; *Hoppe and Russell*, 1983; *Eastwood et al.*, 2004].

[23] Large amplitude magnetic field pulsations have been observed in mature HFAs. The brief interval of significantly elevated magnetic field strength ($\Delta B/B \sim 4$) near 0755 UT in Figure 9 (right) shows what have been termed "magnetic pulsations" [*Thomsen et al.*, 1990]. Magnetic pulsations are a common feature in the quasi-parallel foreshock and have been found to bear a number of similarities to HFAs [*Thomsen et al.*, 1990]. *Thomsen et al.* [1990] suggested that magnetic pulsations are manifestations of the basic physical processes that generate other phenomena at the quasi-parallel shock, such as 30 s electromagnetic waves, shocklets and HFAs. Our observations of small amplitude waves in a proto-HFA, 30 s electromagnetic waves ($\Delta B/B \sim 1$) in a young HFA, and magnetic pulsations in a mature HFA ($\Delta B/B \sim 4$) indicate that they are at early, middle and late (nonlinear)

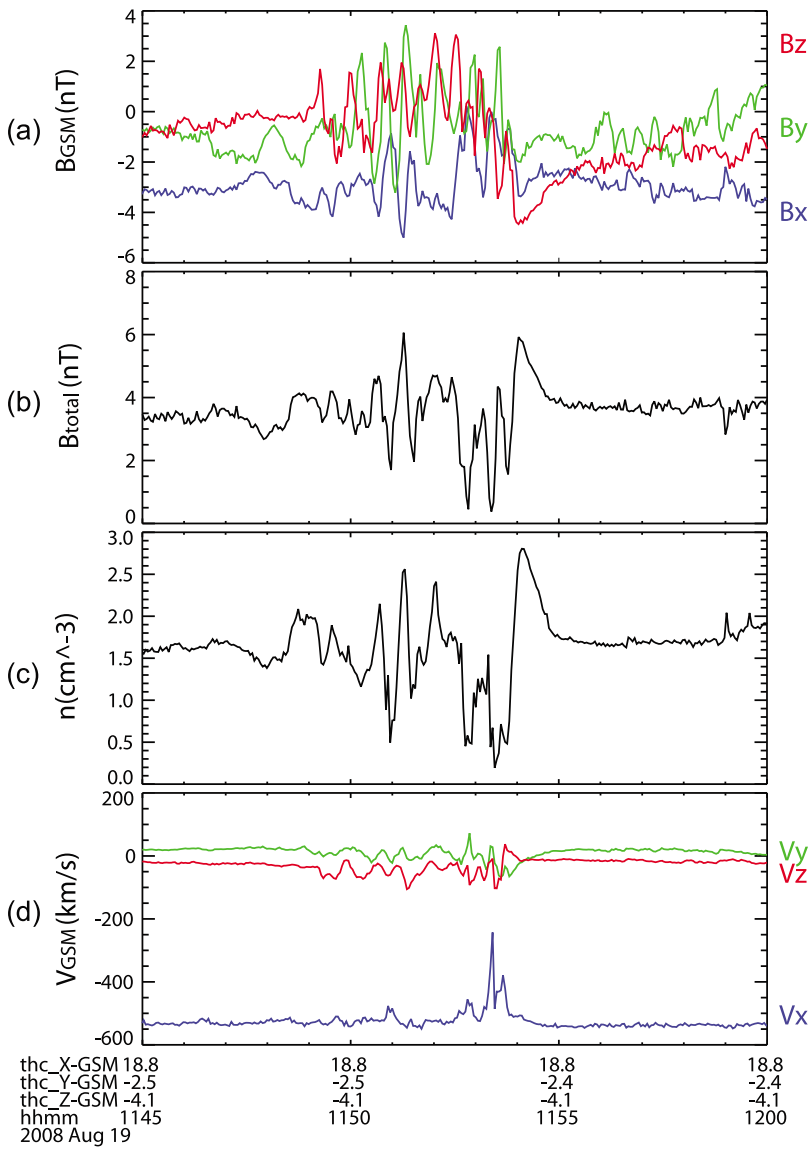

Figure 12. The 30 s period transverse electromagnetic waves inside a young HFA observed by THEMIS C (HFA 5) in Figure 4. (a) Components of the magnetic field in GSM coordinate system, (b) magnetic field magnitude, (c) plasma density (in cm^{-3}), and (d) components of plasma ion flow are shown.

stages of the right-hand resonant instabilities, confirming *Thomsen et al.*'s [1990] suggestion.

[24] Although the right-hand resonant instability has been observed in both the foreshock and HFAs, the significant heating only occurs in HFAs. The reason is that significant heating requires a relative long wave-particle interaction time and a mechanism to focus the particles in the region of interaction. Inward pointing electric fields associated with current sheets play a crucial role in focusing the particles near the current sheet [*Thomsen et al.*, 1993]. Also the development a HFA requires the current sheet to interact with the bow shock for a sufficiently long time interval [*Schwartz et al.*, 2000]. It took the proto-HFA shown in Figure 9 left 110 s to develop into the mature HFA shown in Figure 9 right. Thus only those interplanetary discontinuities with the right orientation (inward pointing electric field, having sufficient time to interact with the bow shock) could generate HFAs and that is why 30s electromagnetic waves and magnetic pulsations are more frequently observed in the foreshock region than HFAs.

3.2.2. Electron Heating

[25] We have shown evidence for electron heating in both proto-HFAs and mature HFAs (Figures 5g, 7e, and 9f). Although electron heating inside mature HFAs has been reported before [e.g., *Schwartz et al.*, 1985], it is not clear how electrons are heated. Enhanced fluctuations driven by kinetic instabilities are a possible source of electron heating in HFAs. Two such possible sources are ion acoustic waves at frequencies below the ion plasma frequency and lower hybrid waves near the lower hybrid frequency. Ion acoustic instabilities need $T_e \gg T_i$ to have strong growth, and are not likely to arise under the conditions of $T_e < T_i$ shown in Figure 6.

[26] On the other hand, the lower hybrid drift instability, driven by density and magnetic field gradients perpendicular

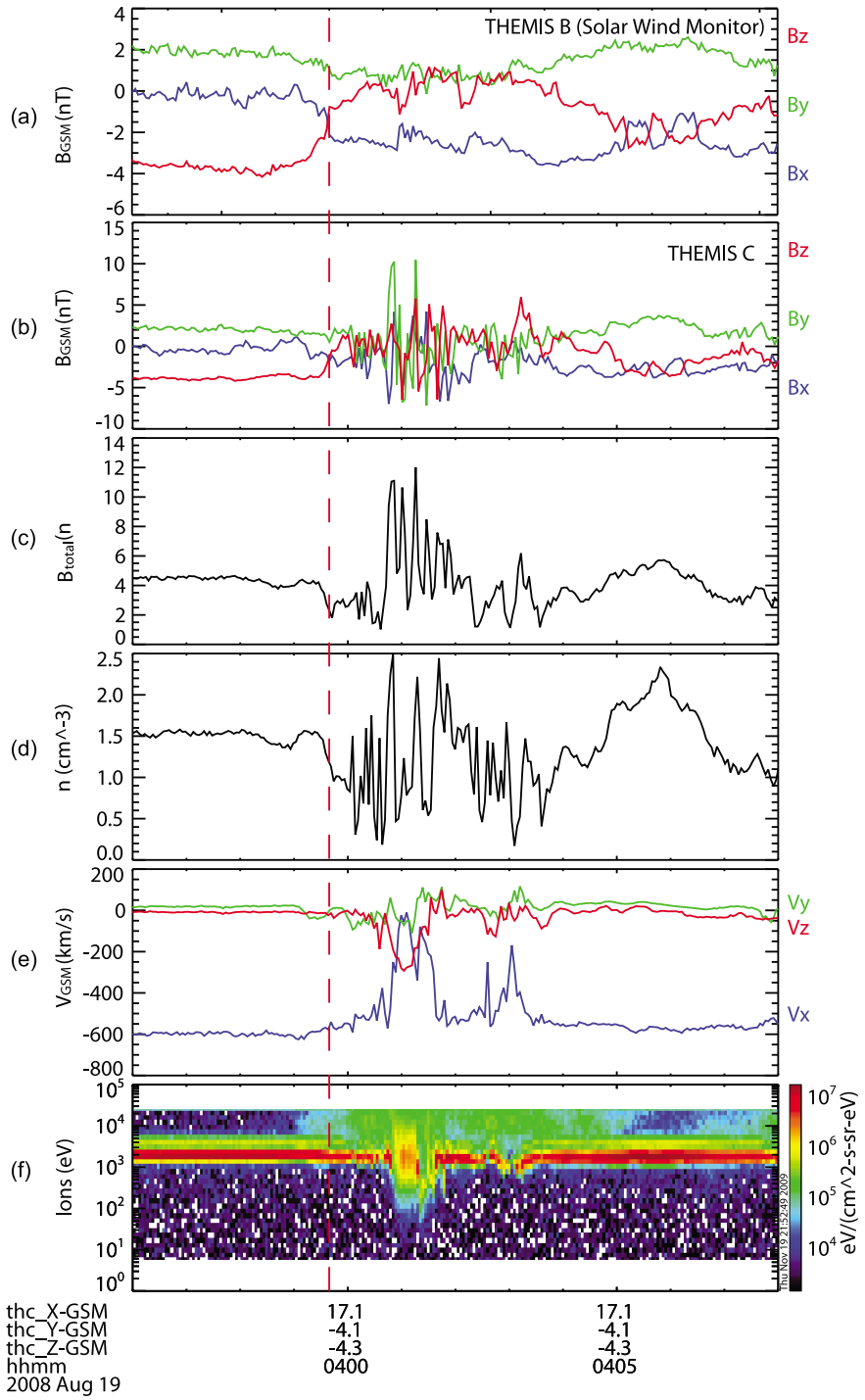

Figure 13. An HFA lying displaced toward the side of the TD with a quasi-parallel bow shock configuration observed by THEMIS C. (a) Time-shifted (~3 min) magnetic field observed by the local solar wind monitor THEMIS B, (b) components of the magnetic field in GSM coordinate system, (c) magnetic field magnitude, (d) plasma density, (e) components of plasma ion flow, and (f) plasma ion spectrum are shown. The vertical red dashed line marks the discontinuity which drove this HFA. The quasi-parallel bow shock configuration on the right-hand side of the TD can be identified by the presence of superthermal particles in Figure 13f.

to the background magnetic field, is enhanced by decreasing T_e/T_i [*Davidson and Krall*, 1977] and therefore is a good candidate for electron heating in HFAs. The fluctuating electric fields of the lower hybrid drift instability are predominantly perpendicular to the background magnetic field [*Davidson and Krall*, 1977], so instability growth leads to electron heating primarily in perpendicular directions, as demonstrated by particle-in-cell simulations [e.g., *Daughton*

et al., 2004]. If this heating is sufficiently strong and $T_{\perp e}/T_{\|e}$ becomes sufficiently greater than unity, this electron temperature anisotropy will drive another growing mode, the whistler anisotropy instability [*Shapiro and Shevchenko*, 1988; *Gary*, 1993]. The resulting enhanced fluctuations scatter the electrons back toward isotropy, and are particularly effective in high-beta plasmas [*Gary and Wang*, 1996]. Thus the combination of the two instabilities provides a scenario in which electrons can be strongly heated in HFAs, and yet be observed to be relatively isotropic, as shown in Figure 7.

3.3. Scale Size of HFAs

[27] The thickness of HFAs in the direction of motion is estimated to be several R_E based on single spacecraft measurements [e.g., *Schwartz et al.*, 1985; *Thomsen et al.*, 1986; *Sibeck et al.*, 1999; *Facskó et al.*, 2009a, 2009b]. However we know little about their extension upstream from the bow shock due to the lack of simultaneous observations of HFAs by multiple spacecraft. As can be seen from Figure 3, THEMIS B (C) was at around 28 (19) R_E, 14 (5) R_E upstream from the bow shock (at 14 R_E). THEMIS B observed four proto-HFAs (Figure 8) which later developed into HFAs 2, 4, 5, and 6 observed by THEMIS C. This indicates that the scale length of HFAs 2, 4, 5, and 6 might exceed 14 R_E, which is surprising given that all previously reported HFAs occurred near the bow shock. Scale lengths of HFAs 1, 3, and 7 should be between 5 and 14 R_E.

3.4. Where Do HFAs Occur? Quasi-Perpendicular or Quasi-Parallel Shock?

[28] As mentioned earlier, where HFAs occur is an outstanding problem. Both simulations and observations show completely different results on whether HFAs occur at quasi-perpendicular or quasi-parallel shocks. Here we show an example of an HFA which is consistent with global hybrid simulation results from *Omidi and Sibeck* [2007].

[29] Figure 13 shows an HFA observed by THEMIS C (HFA 2 in Figure 4). Figure 13a shows the time-shifted (3 min) magnetic field observed by the solar wind monitor, THEMIS B. Figures 13b and 13c show components and magnitude of the magnetic field. Figures 13d–13f show the ion density, velocity components, and spectrum measured by the ESA instrument. The HFA centered at 0401 UT can be identified by the significantly deflected plasma flow (Figure 13e) and greatly heated plasma (illustrated by a broader ion spectrum in Figure 13f). The vertical red dashed line at 0359:40 UT marks the TD discontinuity that generated this HFA. The IMF rotates from duskward and southward to antisunward at the discontinuity. The quasi-parallel bow shock configuration on the right-hand side of the TD can be identified by the presence of the shock-reflected suprathermal (~10 keV) particles in addition to the solar wind particles (~1 keV) in Figure 13f. Clearly, this HFA lies displaced from the TD toward the quasi-parallel bow shock, consistent with *Omidi and Sibeck*'s [2007] result as indicating HFA formation in the quasi-parallel shock region (see Figure 2). In addition, the HFA lies displaced toward the side of the TD with a quasi-parallel bow shock configuration instead of lying centered on the driving IMF TD. This result is completely different with previous observations which showed HFAs lying centered on the driving IMF TD [e.g., *Šafránková et al.*, 2002].

4. Conclusions

[30] A series of seven hot flow anomaly events has been observed by THEMIS C spacecraft 5 R_E upstream from the subsolar bow shock from 0100 to 1300 UT on 19 August 2008. Both young (no shocks at edges, two distinct ion populations) and mature (strong shocks at edges, a single hot ion population) HFAs have been observed. THEMIS B further upstream observed four proto-HFAs (density and magnetic field strength depletion, plasma heating but no flow deflection) which later developed into HFAs observed by THEMIS C. THEMIS observations indicate that electromagnetic right-hand resonant ion beam instabilities are sources of ion heating inside HFAs. Observations of small amplitude resonant ion beam instability ($\Delta B/B < 50\%$) in a proto-HFA, 30s electromagnetic waves ($\Delta B/B \sim 1$) in a young HFA, and magnetic pulsations in a mature HFA ($\Delta B/B \sim 4$) indicate that they are at early, middle and late (nonlinear) stage of the electromagnetic right-hand resonant ion beam instabilities, confirming *Thomsen et al.*'s [1990] suggestion that magnetic pulsations are manifestations of the basic physical processes that generated other phenomena at the quasi-parallel shock, such as 30s electromagnetic waves, shocklets and HFAs. Both young and mature HFAs are associated with strong electromagnetic waves near the lower hybrid frequency (0.1–1 Hz). The lower hybrid waves are the likely source of the electron heating inside HFAs. THEMIS B observations of four proto-HFAs which later developed into HFAs observed by THEMIS C indicate that the scale length of these four HFAs might exceed 14 R_E, and scale lengths of the other three HFAs may be between 5 and 14 R_E. We also present an example of an HFA that lies displaced toward the side of the TD with a quasi-parallel bow shock configuration rather than lying centered on the driving IMF discontinuity, consistent with *Omidi and Sibeck*'s [2007] hybrid simulation results.

[31] **Acknowledgments.** The first author thanks Nick Omidi for helpful discussions. This work is partly supported by NSF grant AGS-0963111.

[32] Philippa Browning thanks Gabor Facsko and another reviewer for their assistance in evaluating this paper.

References

Akimoto, K., D. Winske, S. P. Gary, and M. F. Thomsen (1993), Nonlinear evolution of electromagnetic ion beam instabilities, *J. Geophys. Res.*, *98*, 1419–1433, doi:10.1029/92JA02345.

Angelopoulos, V. (2008), The THEMIS Mission, *Space Sci. Rev.*, *141*, 5–34, doi:10.1007/s11214-008-9336-1.

Auster, H. U., et al. (2008), The THEMIS fluxgate magnetometer, *Space Sci. Rev.*, *141*, 235–264, doi:10.1007/s11214-008-9365-9.

Daughton, W., G. Lapenta, and P. Ricci (2004), Nonlinear evolution of the lower-hybrid drift instability in a current sheet, *Phys. Rev. Lett.*, *93*(10), 105004, doi:10.1103/PhysRevLett.93.105004.

Davidson, R. C., and N. A. Krall (1977), Anomalous transport in high-temperature plasmas with applications to solenoidal fusion systems, *Nucl. Fusion*, *17*, 1313–1372.

Eastwood, J. P., A. Balogh, C. Mazelle, I. Dandouras, and H. Rème (2004), Oblique propagation of 30 s period fast magnetosonic foreshock waves: A Cluster case study, *Geophys. Res. Lett.*, *31*, L04804, doi:10.1029/2003GL018897.

Eastwood, J. P., et al. (2008), THEMIS observations of a hot flow anomaly: Solar wind, magnetosheath, and ground-based measurements, *Geophys. Res. Lett.*, *35*, L17S03, doi:10.1029/2008GL033475.

Facskó, G., K. Kecskeméty, G. Erdős, M. Tátrallyay, P. W. Daly, and I. Dandouras (2008), A statistical study of hot flow anomalies using Cluster data, *Adv. Space Res.*, *41*, 1286–1291, doi:10.1016/j.asr.2008.02.005.

Facskó, G., Z. Németh, G. Erdős, A. Kis, and I. Dandouras (2009a), A global study of hot flow anomalies using Cluster multi-spacecraft measurements, *Ann. Geophys.*, *27*(5), 2057–2076.

Facskó, G., J. G. Trotignon, I. Dandouras, E. A. Lucek, and P. W. Daly (2009b), Study of hot flow anomalies using Cluster multi-spacecraft measurements, *Adv. Space Res.*, *45*, 541–552, doi:10.1016/j.asr.2009.08.011.

Fairfield, D. H. (1969), Bow shock associated waves observed in the far upstream interplanetary medium, *J. Geophys. Res.*, *74*, 3541–3553, doi:10.1029/JA074i014p03541.

Feldman, W. C., R. C. Anderson, S. J. Bame, J. T. Gosling, R. D. Zwickl, and E. J. Smith (1983), Electron velocity distributions near interplantary shocks, *J. Geophys. Res.*, *88*, 9949–9958, doi:10.1029/JA088iA12p09949.

Gary, S. P. (1991), Electromagnetic ion/ion instabilities and their consequences in space plasmas—A review, *Space Sci. Rev.*, *56*, 373–415, doi:10.1007/BF00196632.

Gary, S. P. (1993), *Theory of Space Plasma Microinstabilities*, Cambridge Univ. Press, New York.

Gary, S. P., and J. Wang (1996), Whistler instability: Electron anisotropy upper bound, *J. Geophys. Res.*, *101*, 10,749–10,754, doi:10.1029/96JA00323.

Hoppe, M. M., and C. T. Russell (1983), Plasma rest frame frequencies and polarizations of the low-frequency upstream waves: ISEE 1 and 2 observations, *J. Geophys. Res.*, *88*, 2021–2027, doi:10.1029/JA088iA03p02021.

Lin, Y. (2002), Global hybrid simulation of hot flow anomalies near the bow shock and in the magnetosheath, *Planet. Space Sci.*, *50*, 577–591.

Lucek, E. A., T. S. Horbury, A. Balogh, I. Dandouras, and H. Rème (2004), Cluster observations of hot flow anomalies, *J. Geophys. Res.*, *109*, A06207, doi:10.1029/2003JA010016.

McFadden, J. P., C. W. Carlson, D. Larson, M. Ludlam, R. Abiad, B. Elliott, P. Turin, M. Marckwordt, and V. Angelopoulos (2008), The THEMIS ESA plasma instrument and in-flight calibration, *Space Sci. Rev.*, *141*, 277–302, doi:10.1007/s11214-008-9440-2.

Omidi, N., and D. G. Sibeck (2007), Formation of hot flow anomalies and solitary shocks, *J. Geophys. Res.*, *112*, A01203, doi:10.1029/2006JA011663.

Onsager, T. G., M. F. Thomsen, J. T. Gosling, and S. J. Bame (1990), Observational test of a hot flow anomaly formation mechanism, *J. Geophys. Res.*, *95*, 11,967–11,974, doi:10.1029/JA095iA08p11967.

Onsager, T. G., D. Winske, and M. F. Thomsen (1991), Interaction of a finite-length ion beam with a background plasma: Reflected ions at the quasi-parallel bow shock, *J. Geophys. Res.*, *96*, 1775–1788, doi:10.1029/90JA02008.

Šafránková, J., L. Přech, Z. Němeček, and D. Sibeck (2002), The structure of hot flow anomalies in the magnetosheath, *Adv. Space Res.*, *30*, 2737–2744.

Schwartz, S. J. (1995), Hot flow anomalies near the Earth's bow shock, *Adv. Space Res.*, *15*, 107–116, doi:10.1016/0273-1177(95)00025-A.

Schwartz, S. J., C. P. Chaloner, D. S. Hall, P. J. Christiansen, and A. D. Johnstones (1985), An active current sheet in the solar wind, *Nature*, *318*, 269–271, doi:10.1038/318269a0.

Schwartz, S. J., G. Paschmann, N. Sckopke, T. M. Bauer, M. Dunlop, A. N. Fazakerley, and M. F. Thomsen (2000), Conditions for the formation of hot flow anomalies at Earth's bow shock, *J. Geophys. Res.*, *105*, 12,639–12,650, doi:10.1029/1999JA000320.

Shapiro, V. D., and V. I. Shevchenko (1988), Astrophysical plasma turbulence. Part I., *Astrophys. Space Phys. Rev.*, *6*, 425–546.

Sibeck, D. G., et al. (1999), Comprehensive study of the magnetospheric response to a hot flow anomaly, *J. Geophys. Res.*, *104*, 4577–4594, doi:10.1029/1998JA900021.

Sonnerup, B. U. Ö., and L. J. Cahill Jr. (1967), Magnetopause structure and attitude from Explorer 12 observations, *J. Geophys. Res.*, *72*, 171–183.

Thomas, V. A., and S. H. Brecht (1988), Evolution of diamagnetic cavities in the solar wind, *J. Geophys. Res.*, *93*, 11,341–11,353, doi:10.1029/JA093iA10p11341.

Thomas, V. A., D. Winske, M. F. Thomsen, and T. G. Onsager (1991), Hybrid simulation of the formation of a hot flow anomaly, *J. Geophys. Res.*, *96*, 11,625–11,632, doi:10.1029/91JA01092.

Thomsen, M. F., J. T. Gosling, S. A. Fuselier, S. J. Bame, and C. T. Russell (1986), Hot, diamagnetic cavities upstream from the Earth's bow shock, *J. Geophys. Res.*, *91*, 2961–2973, doi:10.1029/JA091iA03p02961.

Thomsen, M. F., J. T. Gosling, S. J. Bame, K. B. Quest, and C. T. Russell (1988), On the origin of hot diamagnetic cavities near the Earth's bow shock, *J. Geophys. Res.*, *93*, 11,311–11,325, doi:10.1029/JA093iA10p11311.

Thomsen, M. F., J. T. Gosling, S. J. Bame, and C. T. Russell (1990), Magnetic pulsations at the quasi-parallel shock, *J. Geophys. Res.*, *95*, 957–966, doi:10.1029/JA095iA02p00957.

Thomsen, M. F., V. A. Thomas, D. Winske, J. T. Gosling, M. H. Farris, and C. T. Russell (1993), Observational test of hot flow anomaly formation by the interaction of a magnetic discontinuity with the bow shock, *J. Geophys. Res.*, *98*, 15,319–15,330, doi:10.1029/93JA00792.

Tjulin, A., E. A. Lucek, and I. Dandouras (2008), Wave activity inside hot flow anomaly cavities, *J. Geophys. Res.*, *113*, A08113, doi:10.1029/2008JA013333.

Woolliscroft, L. J. C., C. C. Brown, S. J. Schwartz, C. P. Chaloner, and P. J. Christiansen (1986), AMPTE-UKS observations of current sheets in the solar wind, *Adv. Space Res.*, *6*, 89–92, doi:10.1016/0273-1177(86)90017-7.

V. Angelopoulos, Institute of Geophysics and Planetary Physics, Department of Earth and Space Sciences, University of California, Los Angeles, 3845 Slichter Hall, 603 Charles E. Young Dr. E., Los Angeles, CA 90065-1567, USA.

S. P. Gary, Space Science and Applications, Los Alamos National Laboratory, PO Box 1664, MS B241, Los Alamos, NM 87545, USA.

K.-H. Glassmeier, Institute for Geophysics and Extraterrestrial Physics, Technische Universität Braunschweig, Mendelssohnstr. 3, D-38106 Braunschweig, Germany.

D. Larson and J. P. McFadden, Space Sciences Laboratory, University of California, Berkeley, 7 Gauss Way, Berkeley, CA 94720, USA.

D. G. Sibeck, NASA Goddard Space Flight Center, Mail Code 674, Greenbelt, MD 20771, USA.

H. Zhang, Geophysical Institute, University of Alaska Fairbanks, 903 Koyukuk Dr., PO Box 757320, Fairbanks, AK 99775, USA. (hzhang@gi.alaska.edu)

Q.-G. Zong, Center for Atmospheric Research, University of Massachusetts Lowell, 600 Suffolk St., 3rd Floor, Lowell, MA 01854, USA.